Verifying angular-position entanglement by Hardy's paradox with multisetting high-dimensional systems

Dongkai Zhang,[1,2] Xiaodong Qiu,[1] Wuhong Zhang,[1,*] and Lixiang Chen[1,†]

[1]*Department of Physics, Collaborative Innovation Center for Optoelectronic Semiconductors and Efficient Devices, Xiamen University, Xiamen 361005, China*

[2]*College of information Science and Engineering, Fujian Provincial Key Laboratory of Light Propagation and Transformation, Huaqiao University, Xiamen, Fujian 361021, China*

(Received 8 January 2022; accepted 19 May 2022; published 1 June 2022)

High-dimensional entangled states are of crucial importance, as they provide higher channels for quantum information. Angular position, as a continuous variable, provides an infinite Hilbert space theoretically. It is usually represented in discrete bases experimentally because of the convenient modulation of the width of the angular aperture. Thus the combination of the angular apertures will conveniently shape the two photon states. And the entanglement of the two photon states can be naturally demonstrated by Hardy's paradox. Here, by testing Hardy's paradox for two-setting high-dimensional angular subspaces with dimension ranging from 2 to 7 and for multisetting three-dimensional subspaces with setting ranging from 3 to 5, we reveal the high-dimensional entanglement in the angular-position degree of freedom. We show that the high-dimensional angular-position entanglement can yield a much sharper contradiction between the quantum mechanics and classical theories. Our work shows that the angular variable can be considered as an alternative discrete base to provide the high-dimensional entangled states. Thus it may be used as a new platform for quantum information.

DOI: 10.1103/PhysRevA.105.062401

I. INTRODUCTION

Two photons, namely signal photon and idler photon produced by spontaneous parametric down conversion (SPDC), can be entangled in various degrees of freedom, such as time and energy [1,2], position and momentum [3–5], radial position and radial momentum [6], and angular position and orbital angular momentum (OAM) [7–11]. Hitherto, much attention has been paid to the two conjugate variables, i.e., the angular position and OAM, whose correlation is fundamentally different with the other degrees of freedom, since the OAM is a discrete quantum observable of infinite dimension and the angular position is continuous but periodic, and therefore bounded [12–14]. The angular position and OAM are connected by the Fourier transformation [15]. As a result, the optical interference and diffraction effects can be naturally transformed into the angular version, i.e., measurement of the OAM spectrum when a photon field passes through the various angular apertures [16–19]. On the other hand, the demonstration of EPR-Reid criterion sheds new light on exploiting the two special conjugate variables for quantum information, such as the efficient method for sorting both of the OAM and angular modes for quantum information [20], the high-dimensional quantum key distribution scheme [21], and the new way to directly measure the 27-dimensional OAM state vector [22].

Apart from focusing on the exploration of both of these two conjugate variables, photon's OAM, as an independent degree of freedom [23,24], has been paid considerable attention in quantum information science and applications, such as superdense coding [25], quantum teleportation [26], entanglement swapping [27], quantum cryptography [21,28,29], and quantum key distribution [30,31].

In contrast with OAM, the angular-position entanglement has not yet been considered separately. Recent schemes have demonstrated angular two-photon interference in two-dimensional angular two-qubit states [18] and even in high-dimensional angular qudit states [19]. The two-qudit quantum state could be actually represented in the discrete angular-position bases, which suggested that such angular qudit states could possibly be suitable for quantifying the nonlocal feature of entanglement via applicable logical paradox. Here, we exploit the discrete angular-position bases to formulate the general multisetting high-dimensional version of Hardy's paradox to verify its nonlocal feature. In comparison with the Bell-type inequalities [32], Hardy's [33,34] theory was an attempt to demonstrate the nonlocality without inequalities, which gave a more intuitive way to show if the system has quantum entanglement. In the two-dimensional state spaces, Hardy's paradox has been employed to show the entanglement in photon's polarization [35–37], energy time [38], and OAM [39,40]. For high-dimensional systems, a general scenario with multisetting high-dimensional systems was theoretically proposed [41,42] and experimentally demonstrated in OAM subspaces [43] to showcase the high-dimensional quantum correlation. However, the multisetting high-dimensional systems with OAM need complex

*zhangwh@xmu.edu.cn
†chenlx@xmu.edu.cn

entanglement concentration [44] to get the optimal Hardy states. In contrast, the optimal angular-position states are more convenient to produce just by varying the width of the angular aperture. Moreover, the angular-position bases may also provide a high-dimensional Hilbert space by using the small enough angular apertures. Therefore, the above points form the major incentive of our present work to look at how to formulate Hardy's proof with the angular-position states and thus demonstrate the high-dimensional entanglement in the angular-position degree of freedom. Within these advantages, the angular-position states are also more convenient to generate the maximal entangled states [19], which are the crucial quantum resources in some quantum tasks such as the quantum cryptography [21]. In addition, since the sensitivity of the angle sensing can be increased by using multisector entangled states [45], our proposed angular position entangled states just correspond to the special states which may have potential advantages in the quantum remote sensing applications.

II. EXPERIMENTAL SETUP AND RESULTS

Our experimental sketch is shown in Fig. 1(a). In the simplest scenario, a Gaussian pump beam creates photon pairs, namely the signal and idler photons, via the nonlinear process of SPDC. On each hand, Alice (or Bob) takes signal photon (or idler photon) transmitting through d angular slits, as shown in Fig. 1(a). The amplitude transmission function of each of the individual angular slits in the angular aperture is given by [18]

$$A_\alpha(\varphi) = \begin{cases} 1, & p_\alpha - \phi_\alpha/2 < \varphi < p_\alpha + \phi_\alpha/2, \\ 0, & \text{others}, \end{cases} \tag{1}$$

where $\alpha = 1, 2, \ldots, d$ labels the αth angular slit with its angular aperture width ϕ_α and orientation p_α, as illustrated in Fig. 1(b). By adding a linear phase grating with the angular aperture, we get the desired hologram which can be displayed on a spatial light modulater (SLM) to shape the signal or idler photon. The followed single mode fiber (SMF) and the single photon detectors (D_s, D_i) as well as the coincidence circuits are used to ensure the correlation detection of the two photons. It is noted that for signal photon and idler photon passing through the d angular slits, there are in principle d^2 alternative pathways. So it can be denoted by the tensorial product of the angular-position bases that

$$\left|\theta_{\phi_\alpha}^{p_\alpha}\right\rangle_s \otimes \left|\theta_{\phi_\beta}^{p_\beta}\right\rangle_i \quad \text{for} \quad \alpha, \beta = 1, 2, \ldots, d, \tag{2}$$

where $|\theta_{\phi_\alpha}^{p_\alpha}\rangle$, $|\theta_{\phi_\beta}^{p_\beta}\rangle$ denote the states of signal and idler photon after they are passing by the ϕ_α, ϕ_β slit with the direction angle of p_α, p_β. Based on the strong position correlations of the two photons from SPDC, we suppose that only the case of $\alpha = \beta$, i.e., $|\theta_{\phi_\alpha}^{p_\alpha}\rangle_s \otimes |\theta_{\phi_\alpha}^{p_\alpha}\rangle_i$, has the appreciable probabilities. In other words, the signal photon and idler photon are generated at the same angle position in the image plane of the crystal, resulting in the positive correlation of the angular position between the two photons. Therefore, we are allowed to rewrite the d-dimensional angular-position quantum

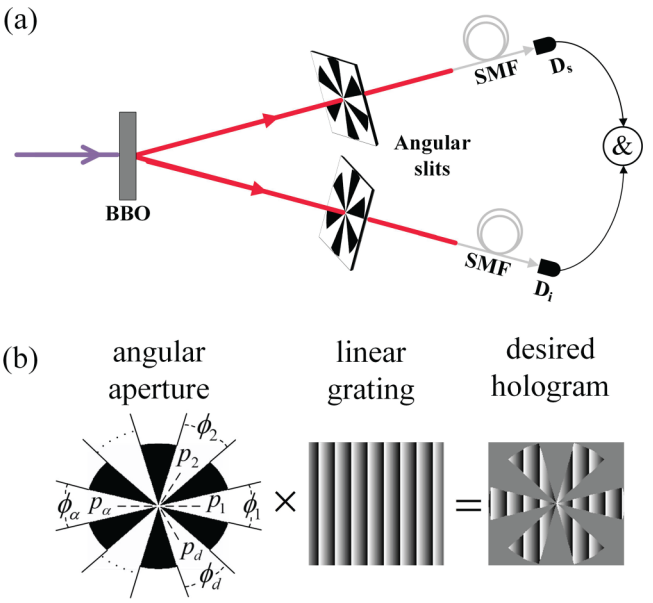

FIG. 1. (a) Schematic of the proposed experimental setup. (b) Angular apertures used to measure the angular-position superposition states. The desired hologram is an example phase pattern programed in SLM.

state as

$$|\Psi\rangle_d = \sum_{\alpha=1}^{d} c_\alpha \left|\theta_{\phi_\alpha}^{p_\alpha}\right\rangle_s \left|\theta_{\phi_\alpha}^{p_\alpha}\right\rangle_i, \tag{3}$$

where c_α indicates the amplitude probability of finding the photon s and the photon i both in the angular slit α. It is noted that the angular-position correlation states from the SPDC are similar with the OAM entangled states, $|\psi\rangle_{\text{SPDC}} = \sum_\ell C_\ell |\ell\rangle_s |-\ell\rangle_i$ [23]. We suppose that Eq. (3) can denote the angular-position entangled states. However, as far as we know, little research has directly demonstrated the entanglement property based on the angular position correlation. We have recently realized Hardy's paradox in a multisetting high-dimensional scheme with OAM [43] and found that the multisetting high dimensional of the Hardy paradox was a good and useful way to demonstrate the high-dimensional entanglement. Compared with the OAM that needs complex entanglement concentration to get the optimal Hardy states, the angular-position states are more convenient to product just by varying the width of the angular aperture based on Eq. (1). For the purpose of testing Hardy's paradox in multisetting high-dimensional angular-position systems, we define k sets of the desired measurements by imparting the different amplitudes to the angular-position eigenmodes as

$$\begin{aligned} \left|A_s^i\right\rangle &= \sum_{\alpha=1}^{d} a_{s,\alpha}^i \left|\theta_{\phi_\alpha}^{p_\alpha}\right\rangle, \\ \left|B_t^j\right\rangle &= \sum_{\beta=1}^{d} a_{t,\beta}^j \left|\theta_{\phi_\beta}^{p_\beta}\right\rangle, \end{aligned} \tag{4}$$

where $i, j \in \{1, 2, \ldots, k\}$ denotes the ith and jth set of measurements; $s, t \in \{1, 2, \ldots, d\}$ labels d possible outcomes for

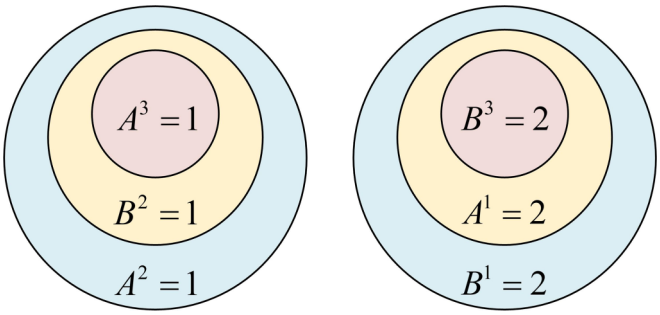

FIG. 2. Venn diagrams for the events of $A^i = 1, 2$ and $B^j = 1, 2$ with $i, j = 1, 2, 3$, satisfy the conditions of (I), (II), and (III). In classical logical, the sets $A^3 = 1$ and $B^3 = 2$, being internal to disjoint sets, cannot intersect, so that (IV) follows immediately.

each set of all of the observable measurements. Within the ith and jth set of measurements, the results satisfy $\langle A_s^i \mid A_{s'}^i \rangle = \delta_{ss'}$ and $\langle B_t^j \mid B_{t'}^j \rangle = \delta_{tt'}$. We first take the two-dimensional angular subspace as an example to demonstrate Hardy's logical structure. For the two-dimensional systems, the observable measurements have only two possible outcomes, i.e., $s, t = 1, 2$. The paradox clarifies that, if observing the following properties in their results, (I) the outcome $A^1 = 1$ and $B^k = 2$ never occurs, i.e., $P(A_1^1, B_2^k) = 0$, (II) the outcome $B^{i-1} = 1$ and $A^{i-1} = 2$ never occurs for all $i = 2, 3, \ldots, k$, i.e., $P(B_1^{i-1}, A_2^{i-1}) = 0$ for $i = 2, 3, \ldots, k$, and (III) the outcome $A^i = 1$ and $B^{i-1} = 2$ never occurs for all $i = 2, 3, \ldots, k$, i.e., $P(A_1^i, B_2^{i-1}) = 0$ for $i = 2, 3, \ldots, k$, then in the classical framework of local hidden-variable theory, if these three properties hold true, they will force the following fourth property: (IV) the outcome $A^k = 1$ and $B^k = 2$ never occurs, i.e., $P(A_1^k, B_2^k) = 0$.

However, quantum mechanics allows the suitable choice of measurements to satisfy (I), (II), and (III), but $P(A_1^k, B_2^k) > 0$. To graphically illustrate the logical structure of Hardy's paradox in a multisetting high-dimensional system, we consider the case $k = 3$ for instance by using the Venn diagrams [40]. The Venn sets associated with the outcomes $A^i = 1, 2$ and $B^j = 1, 2$ for $i, j = 1, 2, 3$ are shown in Fig. 2. We first consider the Venn sets of events $A^2 = 1$. From the property of (II), with $i = 3$, we infer that each time Bob measures B^2, and find $B^2 = 1$. Then if Alice measures A^2, she would certainly find $A^2 = 1$. In other words, the event $B^2 = 1$ implies the event $A^2 = 1$, which is represented by the fact that the Venn set for the event $B^2 = 1$ is internal to the event $A^2 = 1$. Similarly, from the property of (III), with $i = 3$, we infer that the event $A^3 = 1$ implies the event $B^2 = 1$; that is, the Venn set of the event $A^3 = 1$ is internal to the event $B^2 = 1$. Another consideration is the Venn sets of events $B^1 = 2$. From the property of (II), with $i = 2$, we infer that the event $A^1 = 2$ implies the event $B^1 = 2$; that is, the Venn set of the event $A^1 = 2$ is internal to the event $B^1 = 2$. From the property of (I), we infer that the event $B^3 = 2$ implies the event $A^1 = 2$; that is, the Venn set of the event $B^3 = 2$ is internal to the event $A^1 = 2$. Now the property of (III) for $i = 2$ ensures that the events of $A^2 = 1$ and $B^1 = 2$ have no intersection. Therefore, the sets of events $A^3 = 1$ and $B^3 = 2$ cannot intersect either, in which the property of (IV) can be obviously shown as the two discrete Venn sets in Fig. 2. This paradox has been generalized to the high-dimensional situation, where Alice and Bob can obtain k measurements outcome, and the following chain of the probabilities hold [41,42]: $P(A^1 < B^k) = 0$, $P(B^{i-1} < A^{i-1}) = 0$, for $i = 2, 3, \ldots, k$, $P(A^i < B^{i-1}) = 0$, for $i = 2, 3, \ldots, k$, $P(A^k < B^k) > 0$, where $P(A^i < B^j) = \sum_{s<t} P(A_s^i, B_t^j)$ denotes the total joint probability in the case that the measurement outcome of A^i is strictly smaller than B^j.

Then based on Eqs. (3) and (4), the joint probability can be measured as

$$P(A^i < B^j) = \sum_{s=1}^{d-1} \sum_{t=s+1}^{d} \left| \langle A_s^i | \langle B_t^j | \Psi \rangle_d \right|^2. \tag{5}$$

As a result, the maximum Hardy fraction, i.e., the maximum value of the nonlocal probability $P(A^k < B^k)$, can be increased significantly with the increase of the number of the dimension and setting. In order to obtain the maximum value of Hardy's fraction, we use a similar approach as we did in Ref. [43], which is based on the Schmidt decomposition and numerical calculation, to obtain the optimal Hardy states and the desired measurement bases in angular-position subspaces. The obtained optimal Hardy states in two-setting d-dimensional system, i.e., $(2, d)$ scenario, can be denoted as

$$|\psi\rangle_{(2,2)}^{\text{opt}} = 0.9070 |\theta_{100^\circ}^{0^\circ}\rangle_A |\theta_{100^\circ}^{0^\circ}\rangle_B + 0.4211 |\theta_{60^\circ}^{180^\circ}\rangle_A |\theta_{60^\circ}^{180^\circ}\rangle_B, \tag{6a}$$

$$|\psi\rangle_{(2,3)}^{\text{opt}} = 0.8585 |\theta_{158^\circ}^{0^\circ}\rangle_A |\theta_{158^\circ}^{0^\circ}\rangle_B + 0.4040 |\theta_{78^\circ}^{120^\circ}\rangle_A |\theta_{78^\circ}^{120^\circ}\rangle_B + 0.3159 |\theta_{58^\circ}^{240^\circ}\rangle_A |\theta_{58^\circ}^{240^\circ}\rangle_B, \tag{6b}$$

$$|\psi\rangle_{(2,4)}^{\text{opt}} = 0.8263 |\theta_{150^\circ}^{0^\circ}\rangle_A |\theta_{150^\circ}^{0^\circ}\rangle_B + 0.3947 |\theta_{69^\circ}^{115^\circ}\rangle_A |\theta_{69^\circ}^{115^\circ}\rangle_B + 0.3013 |\theta_{48^\circ}^{195^\circ}\rangle_A |\theta_{48^\circ}^{195^\circ}\rangle_B + 0.2657 |\theta_{45^\circ}^{250^\circ}\rangle_A |\theta_{45^\circ}^{250^\circ}\rangle_B, \tag{6c}$$

$$\begin{aligned} |\psi\rangle_{(2,5)}^{\text{opt}} = {} & 0.8024 |\theta_{120^\circ}^{0^\circ}\rangle_A |\theta_{120^\circ}^{0^\circ}\rangle_B + 0.3882 |\theta_{51^\circ}^{90^\circ}\rangle_A |\theta_{51^\circ}^{90^\circ}\rangle_B + 0.2938 |\theta_{44^\circ}^{150^\circ}\rangle_A |\theta_{44^\circ}^{150^\circ}\rangle_B \\ & + 0.2532 |\theta_{43.5^\circ}^{210^\circ}\rangle_A |\theta_{43.5^\circ}^{210^\circ}\rangle_B + 0.2344 |\theta_{45^\circ}^{270^\circ}\rangle_A |\theta_{45^\circ}^{270^\circ}\rangle_B, \end{aligned} \tag{6d}$$

$$\begin{aligned} |\psi\rangle_{(2,6)}^{\text{opt}} = {} & 0.7837 |\theta_{110^\circ}^{0^\circ}\rangle_A |\theta_{110^\circ}^{0^\circ}\rangle_B + 0.3830 |\theta_{52.5^\circ}^{88^\circ}\rangle_A |\theta_{52.5^\circ}^{88^\circ}\rangle_B + 0.2889 |\theta_{37.5^\circ}^{143^\circ}\rangle_A |\theta_{37.5^\circ}^{143^\circ}\rangle_B \\ & + 0.2462 |\theta_{34^\circ}^{190^\circ}\rangle_A |\theta_{34^\circ}^{190^\circ}\rangle_B + 0.2237 |\theta_{32.5^\circ}^{234^\circ}\rangle_A |\theta_{32.5^\circ}^{234^\circ}\rangle_B + 0.2123 |\theta_{34.5^\circ}^{278^\circ}\rangle_A |\theta_{34.5^\circ}^{278^\circ}\rangle_B, \end{aligned} \tag{6e}$$

$$\begin{aligned} |\psi\rangle_{(2,7)}^{\text{opt}} = {} & 0.7683 |\theta_{120^\circ}^{0^\circ}\rangle_A |\theta_{120^\circ}^{0^\circ}\rangle_B + 0.3787 |\theta_{48^\circ}^{90^\circ}\rangle_A |\theta_{48^\circ}^{90^\circ}\rangle_B + 0.2852 |\theta_{31^\circ}^{138^\circ}\rangle_A |\theta_{31^\circ}^{138^\circ}\rangle_B \\ & + 0.2417 |\theta_{25^\circ}^{170^\circ}\rangle_A |\theta_{25^\circ}^{170^\circ}\rangle_B + 0.2173 |\theta_{24^\circ}^{198^\circ}\rangle_A |\theta_{24^\circ}^{198^\circ}\rangle_B + 0.2030 |\theta_{23^\circ}^{226^\circ}\rangle_A |\theta_{23^\circ}^{226^\circ}\rangle_B + 0.1955 |\theta_{26^\circ}^{262^\circ}\rangle_A |\theta_{26^\circ}^{262^\circ}\rangle_B. \end{aligned} \tag{6f}$$

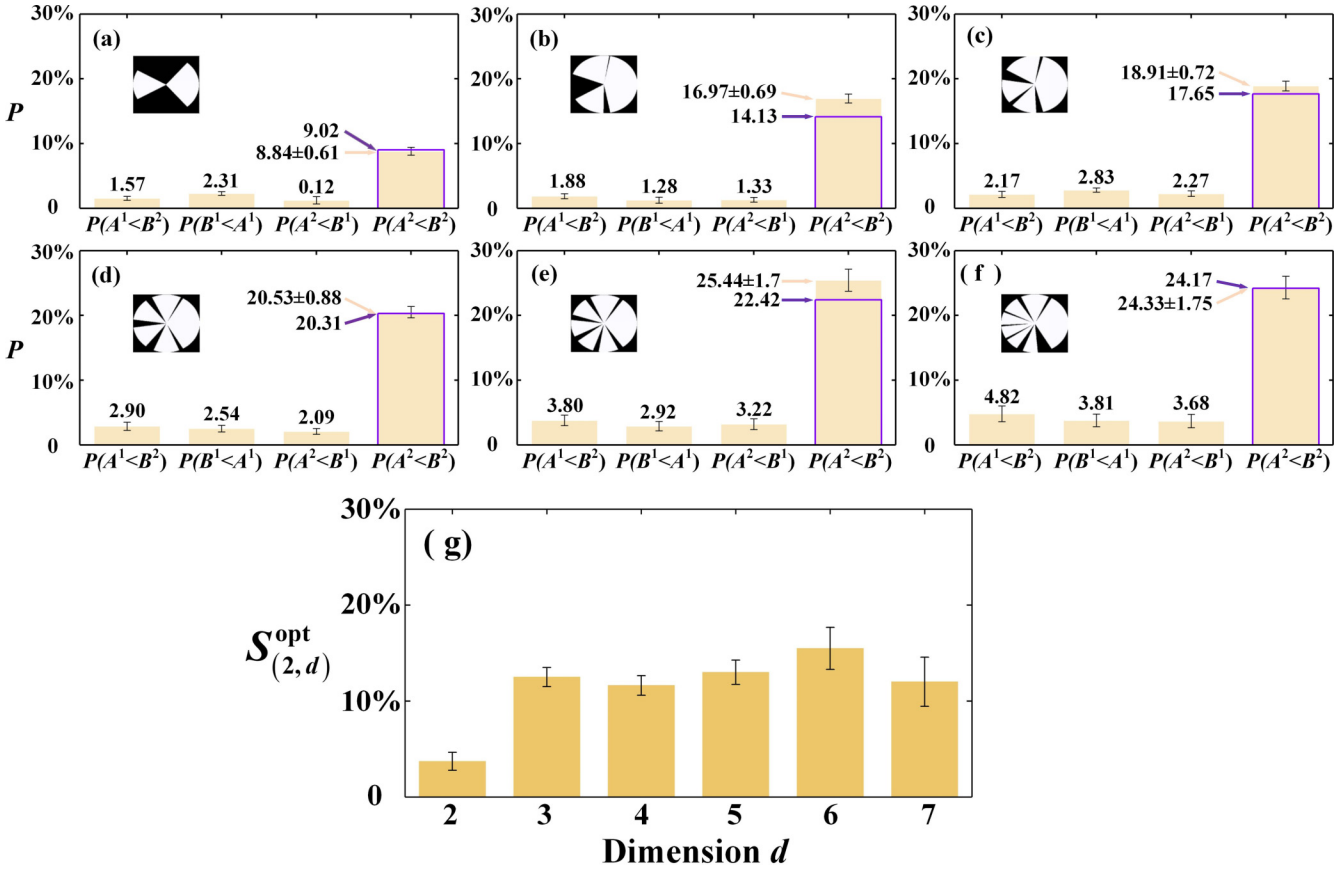

FIG. 3. Experimental results of the two-setting higher-dimensional angular-position subspaces with dimension (a) $d = 2$, (b) $d = 3$, (c) $d = 4$, (d) $d = 5$, (e) $d = 6$, and (f) $d = 7$. The empty bars (purple edges) are the theoretical predictions, while the solid bars (light yellow) are the experimental results. The insets in each graph are the experimental angular apertures used in the $(2, d)$ scenario. (g) The inequality parameter S of the $(2, d)$ scenario.

And the obtained optimal Hardy states in the k-setting three-dimensional system, i.e., $(k, 3)$ scenario, can be written as

$$|\psi\rangle^{\mathrm{opt}}_{(3,3)} = 0.8006|\theta^{0^\circ}_{130^\circ}\rangle_A|\theta^{0^\circ}_{130^\circ}\rangle_B + 0.4578|\theta^{120^\circ}_{70^\circ}\rangle_A|\theta^{120^\circ}_{70^\circ}\rangle_B + 0.3865|\theta^{240^\circ}_{60^\circ}\rangle_A|\theta^{240^\circ}_{60^\circ}\rangle_B, \tag{7a}$$

$$|\psi\rangle^{\mathrm{opt}}_{(4,3)} = 0.7630|\theta^{0^\circ}_{120^\circ}\rangle_A|\theta^{0^\circ}_{120^\circ}\rangle_B + 0.4856|\theta^{120^\circ}_{72^\circ}\rangle_A|\theta^{120^\circ}_{72^\circ}\rangle_B + 0.4267|\theta^{240^\circ}_{60^\circ}\rangle_A|\theta^{240^\circ}_{60^\circ}\rangle_B, \tag{7b}$$

$$|\psi\rangle^{\mathrm{opt}}_{(5,3)} = 0.7366|\theta^{0^\circ}_{118^\circ}\rangle_A|\theta^{0^\circ}_{118^\circ}\rangle_B + 0.5025|\theta^{120^\circ}_{75^\circ}\rangle_A|\theta^{120^\circ}_{75^\circ}\rangle_B + 0.4526|\theta^{240^\circ}_{60^\circ}\rangle_A|\theta^{240^\circ}_{60^\circ}\rangle_B. \tag{7c}$$

Standing on the point of the experimental realization, unlike the other degrees of freedom, such as the OAM that needs mode concentration [43], the optimal Hardy states in the angular-position subspaces are more convenient to produce just by varying the width of the angular slit. Besides, the angular-position bases can also provide a high-dimensional Hilbert space by use of the small enough angular apertures. In our experimental implementation, we first concentrate on the high-dimensional situation. We consider the two-setting Hardy proof for the high-dimensional angular-position subspaces with the dimension d ranging from $d = 2$ to 7. The measurement bases can be obtained based on the given optimal angular-position Hardy states by ranging over all unitary matrices. Interestingly enough, we find the measurement bases are exactly the same as our previous measurement bases in OAM with $(2, d)$ and $(k, 3)$ [43]. This can be explained by the same form of Eq. (3) with the OAM entanglement states.

In an effort to experimentally achieve the maximal probability of the nonlocal events, we vary the width of the angular slits to product the optimal angular-position states. Specially, we preset each of the angular-position bases $|\theta^{p_\alpha}_{\phi_\alpha}\rangle$, $\alpha = 1, 2, \ldots d$, at the width $\phi_\alpha (\phi_\alpha \propto C^2_\alpha)$ and the orientation $p_\alpha = 2\pi\alpha/d$ to measure the weight amplitudes. For each of the weight amplitudes of the angular states, if it is larger (or lower) than the optimal Hardy state, we decrease (or increase) the width ϕ_α and adjust the orientation p_α to ensure that any of them are no overlap. Therefore, the weight amplitudes of each of the angular states in experiment can be equalized with the optimal Hardy states. Then, we load the angular-position superposition states in the SLMs and record the coincidence counts. Our results are shown in Figs. 3(a)–3(f), where the empty bars (purple edges) are the theoretical predictions, while the solid bars (light yellow) are the experimental results. The insets of each graph are the experimental angular apertures used in the $(2, d)$ scenario. It can be seen that

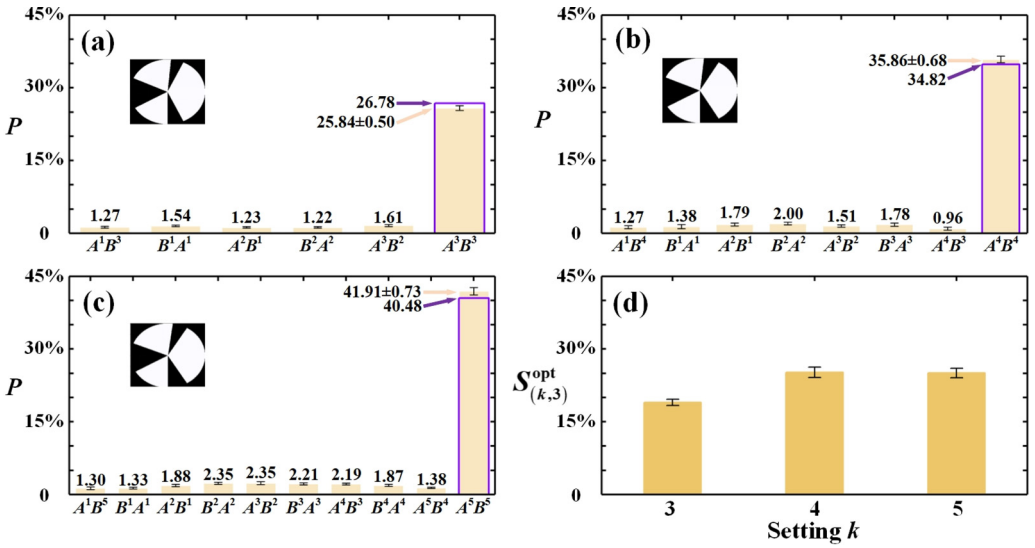

FIG. 4. Experimental results of the multisetting three-dimensional angular-position subspaces with setting (a) $k = 3$, (b) $k = 4$, and (c) $k = 5$. The empty bars (purple edges) are the theoretical values, while the solid bars (light yellow) are the experimental results. A^iB^j and B^jA^i stand for $P(A^i < B^j)$ and $P(B^j < A^i)$, respectively. The insets in each graph are the experimental angular apertures used in the $(k, 3)$ scenario. (g) The inequality parameter S of the $(k, 3)$ scenario.

the optimal probability in two-setting d-dimensional systems, i.e., the $(2, d)$ scenario, can reach $P^{opt}_{(2,2)} = 8.84\% \pm 0.61\%$, $P^{opt}_{(2,3)} = 16.97\% \pm 0.69\%$, $P^{opt}_{(2,4)} = 18.91\% \pm 0.72\%$, $P^{opt}_{(2,5)} = 20.53\% \pm 0.88\%$, $P^{opt}_{(2,6)} = 25.44\% \pm 1.70\%$, and $P^{opt}_{(2,7)} = 24.33\% \pm 1.75\%$. The measurement results are in reasonable agreement with the quantum-mechanical predictions. so it clearly demonstrates our assumptions in Eq. (3). The angular-position entanglement has been verified up to seven dimensions. To take into account the imperfect states, measurements, and detectors, we adopt a statistical measurement procedure to characterize the degree of violation of the localism as

$$S_{(k,d)} = P(A^k < B^k) - \sum_{i=2}^{k} P(A^i < B^{i-1}) - \sum_{i=2}^{k} P(B^{i-1} < A^{i-1}) - P(A^1 < B^k). \quad (8)$$

Following Mermin's theory [46], $S_{k,d} > 0$ can be seen as the entanglement signature of the system, while $S_{k,d} \leqslant 0$ holds true in any local realistic theories. Quantum predictions allow all of the other probabilities to be zero except for the first term of Eq. (8). We can calculate all of the $S_{(2,d)}$ value based on Eq. (8), as illustrated in Fig. 4(g). It can be seen that in two-setting d-dimensional systems, i.e., the $(2, d)$ scenario, the inequality can reach $S^{opt}_{(2,2)} = 3.72\% \pm 0.93\%$, $S^{opt}_{(2,3)} = 12.51\% \pm 1.00\%$, $S^{opt}_{(2,4)} = 11.63\% \pm 1.02\%$, $S^{opt}_{(2,5)} = 13.00\% \pm 1.27\%$, $S^{opt}_{(2,6)} = 15.49\% \pm 2.19\%$, and $S^{opt}_{(2,7)} = 12.01\% \pm 2.56\%$, all of which clearly show the contradiction with the local realism. And thus again our results verify the entanglement in the angular-position degree of freedom.

Our second parts of the experiment further consider the multisetting situation in the angular-position bases. Without loss of generality, we choose the multisetting three-dimensional systems with the setting ranging from $k = 3$ to 5. Following a similar line of the measurement scheme, our results are shown in Figs. 4(a)–4(c). We experimentally obtain the successful probabilities, $P^{opt}_{(3,3)} = 25.84\% \pm 0.50\%$, $P^{opt}_{(4,3)} = 35.86\% \pm 0.68\%$, and $P^{opt}_{(5,3)} = 41.91\% \pm 0.73\%$, respectively. It can be seen that the probabilities of the nonlocal events can be greatly increased with the increase of the number of the setting k, which is consistent with our prediction in Eq. (5). Thus we demonstrate that the angular-position entanglement can be worked even in three dimensions with up to five settings. Again, we show the parameter of S in the $(k, 3)$ scenario in Fig. 4(d), in which the value of S can reach $S^{opt}_{(3,3)} = 18.98\% \pm 0.62\%$, $S^{opt}_{(3,4)} = 25.18\% \pm 1.07\%$, and $S^{opt}_{(3,4)} = 25.06\% \pm 0.98\%$. All of them clearly satisfy the entanglement signature of $S_{k,d} > 0$ and violate the inequality of $S_{(k,d)} \leqslant 0$ by 31, 24, and 26 standard deviations, respectively, and thus confirm the well behavior of the high-dimensional entangled states in the angular-position bases.

III. CONCLUSIONS

In summary, we have shown the experimental tests of the multisetting and high-dimensional Hardy's proof in a two-photon angular-position degree of freedom. Our experimental results demonstrate evidently that the angular variable can be considered as a discrete variable to construct a larger but finite Hilbert space. Thus it is expected to be exploited for further quantum information science and technology. At the same time, our demonstrations of the $(2, d)$ scenario with d ranging from 2 to 7 and the $(k, 3)$ scenario with k ranging from 3 to 5 clearly show the nonlocal quantum effect. In this regard, the multisetting and high-dimensional Hardy proof can be an alternative tool which is used to verify the existence of high-dimensional quantum entanglement. Thus the angular position degree of freedom may inspire a new platform for high-dimensional quantum information technology.

ACKNOWLEDGMENTS

This work is supported by the National Natural Science Foundation of China (Grants No. 12034016, No. 61975169, and No. 11904303), the Fundamental Research Funds for the Central Universities at Xiamen University (Grant No. 20720200074), the Natural Science Foundation of Fujian Province of China for Distinguished Young Scientists (Grant No. 2015J06002), the Youth Innovation Fund of Xiamen (Grant No. 3502Z20206045), and the program for New Century Excellent Talents in University of China (Grant No. NCET-13-0495).

[1] J.-P. W. MacLean, J. M. Donohue, and K. J. Resch, Direct Characterization of Ultrafast Energy-Time Entangled Photon Pairs, Phys. Rev. Lett. **120**, 053601 (2018).

[2] L. K. Shalm, D. R. Hamel, Z. Yan, C. Simon, K. J. Resch, and T. Jennewein, Three-photon energy-time entanglement, Nat. Phys. **9**, 19 (2013).

[3] J. C. Howell, R. S. Bennink, S. J. Bentley, and R. W. Boyd, Realization of the Einstein-Podolsky-Rosen Paradox Using Momentum- and Position-Entangled Photons from Spontaneous Parametric Down Conversion, Phys. Rev. Lett. **92**, 210403 (2004).

[4] P. Moreau, F. Devaux, and E. Lantz, Einstein-Podolsky-Rosen Paradox in Twin Images, Phys. Rev. Lett. **113**, 160401 (2014).

[5] C. Perumangatt, A. Lohrmann, and A. Ling, Experimental conversion of position correlation into polarization entanglement, Phys. Rev. A **102**, 012404 (2020).

[6] L. Chen, T. Ma, X. Qiu, D. Zhang, W. Zhang, and R. W. Boyd, Realization of the Einstein-Podolsky-Rosen Paradox Using Radial Position and Radial Momentum Variables, Phys. Rev. Lett. **123**, 060403 (2019).

[7] J. Leach, B. Jack, J. Romero, A. K. Jha, A. M. Yao, S. Franke-Arnold, D. G. Ireland, R. W. Boyd, S. M. Barnett, and M. J. Padgett, Quantum correlations in optical angle-orbital angular momentum variables, Science **329**, 662 (2010).

[8] Z.-Q. Zhou, Y.-L. Hua, X. Liu, G. Chen, J.-S. Xu, Y.-J. Han, C.-F. Li, and G.-C. Guo, Quantum Storage of Three-Dimensional Orbital-Angular-Momentum Entanglement in a Crystal, Phys. Rev. Lett. **115**, 070502 (2015).

[9] T. S. Yang, Z. Q. Zhou, Y. L. Hua, X. Liu, Z. F. Li, P. Y. Li, Y. Ma, C. Liu, P. J. Liang, X. Lo, Y. X. Xiao, J. Hu, C.-F. Li, and G.-C. Guo, Multiplexed storage and real-time manipulation based on a multiple degree-of-freedom quantum memory, Nat. Commun. **9**, 3407 (2018).

[10] N. Uribe-Patarroyo, A. Fraine, D. S. Simon, O. Minaeva, and A. V. Sergienko, Object Identification Using Correlated Orbital Angular Momentum States, Phys. Rev. Lett. **110**, 043601 (2013).

[11] B. C. Hiesmayr, M. J. A. de Dood, and W. Löffler, Observation of Four-Photon Orbital Angular Momentum Entanglement, Phys. Rev. Lett. **116**, 073601 (2016).

[12] S. Franke-Arnold, S. M. Barnett, E. Yao, J. Leach, J. Courtial, and M. Padgett, Uncertainty principle for angular position and angular momentum, New J. Phys. **6**, 103 (2004).

[13] E. Yao, S. Franke-Arnold, J. Courtial, S. Barnett, and M. Padgett, Fourier relationship between angular position and optical orbital angular momentum, Opt. Express **14**, 9071 (2006).

[14] J. B. Götte, S. Franke-Arnold, and S. M. Barnett, Angular EPR paradox, J. Mod. Opt. **53**, 627 (2006).

[15] A. K. Jha, B. Jack, E. Yao, J. Leach, R. W. Boyd, G. S. Buller, S. M. Barnett, S. Franke-Arnold, and M. J. Padgett, Fourier relationship between the angle and angular momentum of entangled photons, Phys. Rev. A **78**, 043810 (2008).

[16] B. Jack, M. Padgett, and S. Franke-Arnold, Angular diffraction, New J. Phys. **10**, 103013 (2008).

[17] L. Chen, J. Leach, B. Jack, M. J. Padgett, S. Franke-Arnold, and W. She, High-dimensional quantum nature of ghost angular Young's diffraction, Phys. Rev. A **82**, 033822 (2010).

[18] A. K. Jha, J. Leach, B. Jack, S. Franke-Arnold, S. M. Barnett, R. W. Boyd, and M. J. Padgett, Angular Two-Photon Interference and Angular Two-Qubit States, Phys. Rev. Lett. **104**, 010501 (2010).

[19] G. Puentes, High-dimensional angular two-photon interference and angular qudit states, OSA Continuum **3**, 1616 (2020).

[20] M. Mirhosseini, M. Malik, Z. Shi, and R. W. Boyd, Efficient separation of the orbital angular momentum eigenstates of light, Nat. Commun. **4**, 2781 (2013).

[21] M. Mirhosseini, O. S. Magaña-Loaiza, M. N. O'Sullivan, B. Rodenburg, M. P. J. Lavery, M. J. Padgett, D. J. Gauthier, and R. W. Boyd, High-dimensional quantum cryptography with twisted light, New J. Phys. **17**, 033033 (2015).

[22] M. Malik, M. Mirhosseini, M. P. J. Lavery, J. Leach, M. J. Padgett, and R. W. Boyd, Direct measurement of a 27-dimensional orbital-angular-momentum state vector, Nat. Commun. **5**, 3115 (2014).

[23] A. Mair, A. Vaziri, G. Weihs, and A. Zeilinger, Entanglement of the orbital angular momentum states of photons, Nature (London) **412**, 313 (2001).

[24] D. Giovannini, F. M. Miatto, J. Romero, S. M. Barnett, J. P. Woerdman, and M. J. Padgett, Determining the dimensionality of bipartite orbital-angular-momentum entanglement using multi-sector phase masks, New J. Phys. **14**, 073046 (2012).

[25] J. T. Barreiro, T.-C. Wei, and P. G. Kwiat, Beating the channel capacity limit for linear photonic superdense coding, Nat. Phys. **4**, 282 (2008).

[26] X.-L. Wang, X.-D. Cai, Z.-E. Su, M.-C. Chen, D. Wu, L. Li, N.-L. Liu, C.-Y. Lu, and J.-W. Pan, Quantum teleportation of multiple degrees of freedom of a single photon, Nature (London) **518**, 516 (2015).

[27] Y. Zhang, M. Agnew, T. Roger, F. S. Roux, T. Konrad, D. Faccio, J. Leach, and A. Forbes, Simultaneous entanglement swapping of multiple orbital angular momentum states of light, Nat. Commun. **8**, 632 (2017).

[28] S. Gröblacher, T. Jennewein, A. Vaziri, G. Weihs, and A. Zeilinger, Experimental quantum cryptography with qutrits, New J. Phys. **8**, 75 (2006).

[29] A. Sit, F. Bouchard, R. Fickler, J. Gagnon-Bischoff, H. Larocque, K. Heshami, D. Elser, C. Peuntinger, K. Günthner, B. Heim, C. Marquardt, G. Leuchs, R. W. Boyd, and E. Karimi, High-dimensional intracity quantum cryptography with structured photons, Optica **4**, 1006 (2017).

[30] M. Mafu, A. Dudley, S. Goyal, D. Giovannini, M. McLaren, M. J. Padgett, T. Konrad, F. Petruccione, N. Lutkenhaus, and A. Forbes, Higher-dimensional orbital-angular-momentum-based quantum key distribution with mutually unbiased bases, Phys. Rev. A **88**, 032305 (2013).

[31] F. Bouchard, K. Heshami, D. England, R. Fickler, R. W. Boyd, B.-G. Englert, L. L. Sánchez-Soto, and E. Karimi, Experimental investigation of high-dimensional quantum key distribution protocols with twisted photons, Quantum **2**, 111 (2018).

[32] J. S. Bell, On the Einstein-Podolsky-Rosen paradox, Phys. Phys. Fiz. **1**, 195 (1964).

[33] L. Hardy, Quantum Mechanics, Local Realistic Theories, and Lorentz-Invariant Realistic Theories, Phys. Rev. Lett. **68**, 2981 (1992).

[34] L. Hardy, Nonlocality for Two Particles without Inequalities for Almost All Entangled States, Phys. Rev. Lett. **71**, 1665 (1993).

[35] G. Di Giuseppe, F. DeMartini, and D. Boschi, Experimental test of the violation of local realism in quantum mechanics without Bell inequalities, Phys. Rev. A **56**, 176 (1997).

[36] Y. H. Luo, H. Y. Su, H. L. Huang, X. L. Wang, T. Yang, L. Li, N. L. Liu, J. L. Chen, C. Y. Lu, and J. W. Pan, Experimental test of generalized Hardy's paradox, Sci. Bull. **63**, 1611 (2018).

[37] M. Yang, H. X. Meng, J. Zhou, Z. P. Xu, Y. Xiao, K. Sun, J. L. Chen, J. S. Xu, C. F. Li, and G. C. Guo, Stronger Hardy-type paradox based on the Bell inequality and its experimental test, Phys. Rev. A **99**, 032103 (2019).

[38] G. Vallone, I. Gianani, E. B. Inostroza, C. Saavedra, G. Lima, A. Cabello, and P. Mataloni, Testing Hardy's nonlocality proof with genuine energy-time entanglement, Phys. Rev. A **83**, 042105 (2011).

[39] L. Chen and J. Romero, Hardy's nonlocality proof using twisted photons, Opt. Express **20**, 21687 (2012).

[40] E. Karimi, F. Cardano, M. Maffei, C. de Lisio, L. Marrucci, R. W. Boyd, and E. Santamato, Hardy's paradox tested in the spin-orbit Hilbert space of single photons, Phys. Rev. A **89**, 032122 (2014).

[41] J. L. Chen, A. Cabello, Z. P. Xu, H. Y. Su, C. Wu, and L. C. Kwek, Hardy's paradox for high-dimensional systems, Phys. Rev. A **88**, 062116 (2013).

[42] H. X. Meng, J. Zhou, Z. P. Xu, H. Y. Su, T. Gao, F. L. Yan, and J. L. Chen, Hardy's paradox for multisetting high-dimensional systems, Phys. Rev. A **98**, 062103 (2018).

[43] D. Zhang, X. Qiu, T. Ma, W. Zhang, and L. Chen, Orbital-angular-momentum-based experimental test of Hardy's paradox for multisetting and multidimensional systems, Phys. Rev. A **101**, 053821 (2020).

[44] C. Bennett, H. Bernstein, S. Popescu, and B. Schumacher, Concentrating partial entanglement by local operations, Phys. Rev. A **53**, 2046 (1996).

[45] V. D'Ambrosio, N. Spagnolo, L. Del Re, S. Slussarenko, Y. Li, L. C. Kwek, L. Marrucci, S. P. Walborn, L. Aolita, and F. Sciarrino, Photonic polarization gears for ultra-sensitive angular measurements, Nat. Commun. **4**, 2432 (2013).

[46] N. D. Mermin, Quantum mysteries refined, Am. J. Phys. **62**, 880 (1994).